The American Journal of Human Genetics, Volume *100*

Supplemental Data

PLAA Mutations Cause a Lethal Infantile Epileptic Encephalopathy by Disrupting Ubiquitin-Mediated Endolysosomal Degradation of Synaptic Proteins

Emma A. Hall, Michael S. Nahorski, Lyndsay M. Murray, Ranad Shaheen, Emma Perkins, Kosala N. Dissanayake, Yosua Kristaryanto, Ross A. Jones, Julie Vogt, Manon Rivagorda, Mark T. Handley, Girish R. Mali, Tooba Quidwai, Dinesh C. Soares, Margaret A. Keighren, Lisa McKie, Richard L. Mort, Noor Gammoh, Amaya Garcia-Munoz, Tracey Davey, Matthieu Vermeren, Diana Walsh, Peter Budd, Irene A. Aligianis, Eissa Faqeih, Alan J. Quigley, Ian J. Jackson, Yogesh Kulathu, Mandy Jackson, Richard R. Ribchester, Alex von Kriegsheim, Fowzan S. Alkuraya, C. Geoffrey Woods, Eamonn R. Maher, and Pleasantine Mill

Supplemental Note: Case Reports

The first three families containing children with a severe neurodevelopmental disorder were independently ascertained and investigated. The final overarching diagnosis was of a novel disorder, PLAA-associated neurodevelopmental disorder (PLAAND), but the initial clinical diagnoses were Acrocallosal-like syndrome in Family A, PEHO syndrome in Family B, and PEHO-like syndrome in Family C. The inheritance pattern in all three families appeared autosomal recessive; males and females were equally affected, there were normal siblings, the parents had no features of the condition, and parents were first cousins. All families were of Pakistani origin, but not known to be related. A subsequent family carrying the c.68dupG:p.(Leu24Profs*55) mutation was identified in a Middle Eastern cohort of primary microcephaly with seizures patients (Family D). The study had research ethics approval from South Birmingham and Cambridge Local Research Ethics Committees, or from KFSHRC IRB.

Family A comprised a large consanguineous family with five affected individuals, from two sibships (see Figure S1):

The male proband (case A-IV-6) was born at term by emergency Caesarean section because of fetal distress following a pregnancy complicated by polyhydramnios from 34 weeks. He was in good condition with Apgar scores of 5 at one minute and 9 at five minutes and normal growth parameters. He was admitted to the neonatal unit because of feeding difficulties and was noted to have significant neurological abnormalities with truncal hypotonia, very stiff extended limbs with increased tone and he was unable to suck or swallow. Hirsutism, a variety of craniofacial dysmorphisms including a short nose, long philtrum, high palate, low set ears, bilateral single palmar creases and postaxial polydactyly of the left hand and right foot were noted. Cranial ultrasound imaging showed a large central cystic defect between the lateral ventricles and superior to 3rd ventricle. An initial eye assessment found the eyes to be normal but small, however abnormal fundal pigment was later noted. He was found to have congenital hypothyroidism. He continued to feed poorly and developed abnormal movements, which were treated with phenobarbitone. An EEG was immature but there were no other features of note. He died at 12 days following episodes of recurrent profound apnoea.

Subsequently a second affected male sibling (case A-IV-7) was born by forceps delivery. Antenatally a cystic lesion lying superior to the third ventricle thought to represent a large

cavum was identified on foetal MRI. He had Apgar scores of 5 at one minute and 9 at five minutes. He required facial oxygen and was transferred to the neonatal unit with respiratory distress. He had truncal hypotonia, stiffness of the limbs and an inability to suck or swallow. He had similar facial dysmorphic features to case A-IV-6 and a mildly receding forehead, low set posteriorly rotated ears, a prominent sharp cupid's bow lip, a thin vermillion border, a very flat philtrum, a high palate, micrognathia, long fingers and bilateral single palmar creases, left unilateral postaxial polydactyly and a bulbous right 5th toe. Birth weight, length and head circumference were within the normal range however his head circumference had fallen from the 50 centile to the 9 centile by age 5 months. He had puffy feet. He had episodes of apnoea and required tube feeding. He developed optic atrophy and made no developmental progress. A brain MRI scan at 1 week of age was reported as showing a thin intact corpus callosum, delayed myelination, mildly dilated occipital and temporal horns of the lateral ventricles and a simple immature overall gyral pattern particularly frontally, a large cavum septum pellucidum and vergae. He had recurrent pneumonia and died at 16 months of age.

A third sibling (case A-IV-8) was born after an uneventful pregnancy. She did not have polydactyly but her facial appearance and neurodevelopment were similar to her brothers. At 9 months of age her weight was on the 3 centile and her head circumference and length were below the 3rd centile. She could not fix and follow and she had horizontal pendular nystagmus and bilateral optic atrophy. Her hearing was normal. She developed seizures from age 2 years and she died 4 months later with respiratory distress. Her brain MRI scan (at three months) showed a thin intact corpus callosum, delayed myelination, large ventricles with moderate cavum septum pellucidum and CSF spaces, with irregularity/mildly dysplastic outline with the right lateral ventricle being larger than the left (**Fig.1A-C**). Overall the gyral pattern was slightly simple/immature. A full metabolic screen and karyotype was normal.

The affected fourth sibling (case A-IV-10) was a male. In utero his activity was reported to be normal and foetal MRI brain imaging was normal. He was born at 35 weeks of pregnancy in good condition and with normal growth parameters. He had central hypotonia and peripheral hypertonia. He was unable to suck or swallow. He required nasogastric tube feeds and treatment for gastro-oesophageal reflux. At a corrected age of 5 months he was tolerating nasogastric feeds and he had intermittent apnoeas which responded to stimulation. He had nystagmus and roving eye movements. He could fix but

not follow with his eyes. His eyes appeared structurally normal on ophthalmological assessment. Facially he had bitemporal narrowing and full cheeks. He had thick eyebrows. His ears were low set and posteriorly rotated with vertical earlobe creases. He had swelling on the dorsum of his hands and feet and hirsutism. His weight was on the 9 centile and his head circumference was on the 0.4-2 centile. An EEG had features of an epileptic encephalopathy and he was treated with anticonvulsants from the age of a year. At 14 months of age the apneas were less frequent and his stiffness was reduced with baclofen. He had little spontaneous movement and had made no developmental progress. Brain MRI scan at three weeks of age reported large cavum septum pellucidum/cavum vergae, simplified gyral pattern (more affected anteriorly), diffusely increased T2-signal in white matter throughout, thin corpus callosum and enlargement of the trigones and occipital horns, consistent with colcocephaly. He died following a chest infection at the age of 22 months.

A female first cousin (case A-IV-1) to these children whose parents were also first cousins was reported to have the same condition. She was born at 42 weeks of pregnancy with normal growth parameters. She was readmitted on day 8 because of poor feeding due to a poor suck and was treated for gastro-oesophageal reflux. She continued to have a poor feeding and was mainly tube fed. She was noted to have truncal hypotonia and limb hypertonia with clenched hands. She had episodes of suspected seizures with stiffening and clenching of the fists, flickering of the eyes and cyanosis. She had a similar facial appearance, a left tragus ear tag, single palmar creases and 2/3 toe syndactyly. Her left renal pelvis was also dilated. Her EEG was abnormal and her MRI (aged three weeks: **Fig. 1D,E**) showed a delayed gyral pattern more pronounced anteriorly with brain development consistent with 34 weeks gestation with a moderate sized cavum septum pellucidum/cavum vergae, dilatation of the trigones and occipital horns (colcocephaly), diffuse thinning of the corpus callosum and increased white matter signal. At 10 months of age her weight was 7.6 kg on the 9-25 centile, her length was 59 cm below the 0.4 centile and her head circumference was 41.4 cm on the 2 centile. She had severe global delay. She would cry and gurgle loudly. She had become increasingly hypertonic with increased tone and brisk limb reflexes. She had contractures of the wrists and ankles. She was fully tube fed and on treatment for gastro-oesophageal reflux. Episodes of stiffening associated with blue lips became less frequent. She had impaired visual responsiveness

with scanning eye movements and sometimes rapid nystagmus. She developed acute respiratory failure secondary to a chest infection and died age 14 months.

The second and third families contained individuals with clinical features of the neurodevelopmental disorder PEHO (progressive encephalopathy with oedema, hypsarrhythmia, and optic atrophy) syndrome. In Family B the oldest sibling had died but, by history, was likely affected (but clinical details were not available and the child is not included in the summary clinical description). One of six subsequent children was affected (case B-III-1). The parents were Kashmiri in origin and were first cousins. The affected son was born at term after a normal pregnancy. He was normal at birth, left hospital, but then presented in the first week of life with fits, was found to be hypertonic, to have oedema restricted to the dorsum of his hands and feet, and to have deep set eyes and dysplastic finger and toe nails. The seizures continued until age 5 months and then lessened (not thought to be related to medication induced). Secondary microcephaly developed (head circumference was normal at birth but <-2SD at 14 months) and it became clear that he had severe neurodevelopmental delay. Over the first year of life his fingers and toes became noticeably overlapped and he held his plantar flexed, but this was not a fixed deformity. Roving eye movement developed in the first three months, and it was clear by six months that he had gross visual impairment; mild optic atrophy was noted at six months of age. Brain imaging showed a simplified gyral pattern most evident in the frontal lobes, and that the cerebellum was of slightly reduced size. He died at 5 years of age of pneumonia, having made no developmental progress.

In Family C the affected child (case C-III-1) was the third born after two unaffected siblings to consanguineous parents (first cousins) originating from Pakistan. His pregnancy and delivery were normal but he developed fits on the first day, which proved difficult to control. Over the first year a progressive spastic paraplegia became apparent. The dorsum of his feet (but not his hands) had always been swollen, and he also had a coarse facial appearance, arched eyebrows, deep set eyes, synophrys, and long digits; the fingers became progressively more flexed with time. Whilst the head circumference was normal at birth secondary microcephaly was evident by one year. An EEG was very abnormal with hypsarrhythmia. Brain imaging by MRI revealed bilateral pachygyria, a small corpus callosum, small cerebellum and diffuse white matter changes. He died at 6 years of repeated pneumonias, and had also made no developmental progress.

In Family D, the father had two older brothers who had died from a similar clinical condition to case D-VIII-1, although the details are not included here. The affected individual D-VIII-1 was born full term but needed immediate ventilation. He had poor Apgar scores and respiratory acidosis. He had subtle facial dysmorphia (bulbous nose, large ears, and long philtrum) and 3-limb postaxial polydactyly. His birth weight was 2.3 kg, length 55cm and OFC 30.2cm. On 1st day postnatal, he developed repeated tonic-clonic seizures associated with tachycardia and apneic episodes which required increasing doses of keppra. An EEG done on the 2nd day revealed ripples of sleep spindles centrally predominant. Frequent negative Rolandic sharp waves and fronto-central sharp waves were encountered independently in both right and left fronto-central regions. Continuity of sharp waves constituting electrographic seizures were also noted. In addition, electro-clinical seizures were manifested with hyper-rhythmic discharges that emanated from the right frontal and centro-occipital regions. His initial brain CT showed diffuse bilateral symmetrical and significant reduction in the attenuation of the white matter. A brain MRI done at 20 days showed abnormal gyration and sulcation of both cerebral hemispheres, more pronounced at the level of the frontal lobes. In addition, there was prominent T2 hyperintensity. The echocardiography showed small VSD and ASD-II. The baby transferred to another hospital at the 2nd month of life with partially controlled seizure on oral pyridoxine and keppra. The weight 3.01 kg and head circumference 32.5 cm. The baby had several bouts of chest infections and died at 10 months of life.

To define the molecular basis of the autosomal recessively inherited neurodevelopmental disorder in Family A, genome-wide SNP genotyping was undertaken by Affymetrix SNP arrays with DNA from each of the four affected individuals (10k SNP arrays in case A-IV-6 and A-IV-7 and 250k SNP arrays in A-IV-1 and A-IV-8). Initially 6 areas of homozygosity were identified, however further analysis using microsatellite markers in the extended family revealed a single ~14Mb overlapping region of autozygosity on chromosome 9 between D9S235 and D9S1868 (maximum 2-point LOD score was 3.02). Candidate gene analysis was performed and a c.68G>T missense substitution (p.Gly23Val) was identified within the *PLAA* gene and shown to segregate with disease status in the family. This variant was not found in the Exome Variant Server, 1000 Genomes or ExAc databases and was also not detected in 3000 ethnically matched control chromosomes (data not shown). Subsequently whole exome sequencing was performed in

an affected child from family A and no other candidate pathogenic rare variants were detected within the candidate target region (data not shown).

In parallel with investigations performed in Family A, exome analysis was performed on 27 families referred with a clinical diagnosis of PEHO or PEHO-like syndrome and a subanalysis of 12 consanguineous families within the cohort revealed that the probands from Families B and C both carried the same homozygous *PLAA* c.68G>T missense substitution. (Each individual bore a further 5-10 potential pathogenic homozygous mutations within homozygous regions>2cM, but none were shared between the two families). The c.68G>T *PLAA* mutation was confirmed by Sanger sequencing, and segregated as expected for an autosomal recessive disease in each family. Review of the other 25 PEHO/PEHO-like families found no further families with potential bi-allelic *PLAA* mutations. Subsequently, homozygosity mapping and exome sequencing of a primary microcephaly pedigree (Family D) revealed that case D-VIII-1 had a homozygous mutation in *PLAA* :c.68dupG:p.(Leu24Profs*55).

To determine if the G23V mutation was recurrent or ancestral, the genomic region surrounding the c.68G>T *PLAA* mutation was analysed in all three families. In each affected individual there was a region of homozygosity >3cM/3Mb. No further pathogenic mutations were found within this region on re-analysis. Within the 3cM region, and centred on the homozygous mutation, was a 1cM/1Mb region of concordant homozygosity shared between all affected individuals. This result strongly suggests that all three families were distantly related, and that the mutation was ancestral rather than a recurrent mutation (Table S2).

Figure S1: Pedigrees of PLAAND families.

Related to **Figure 1.** Pedigrees of 4 families with identified homozygous *PLAA* mutations. Squares represent males and circles represent females. Filled symbols represent affected individuals. Unaffected individuals who were genotyped for *PLAA* are represented as black dots in the pedigree symbols. For family A, affected individuals who were genotyped as homozygous for the *PLAA* c.[68G>T] mutation are represented as white dots in the pedigree symbols. For family B and C, "affected only" pedigrees are shown, such that unaffected siblings have not been included but have been described in the extended clinical details. For families B, C and D, identified homozygous *PLAA* mutations are shown below the affected.

FAMILY A
PAKISTAN

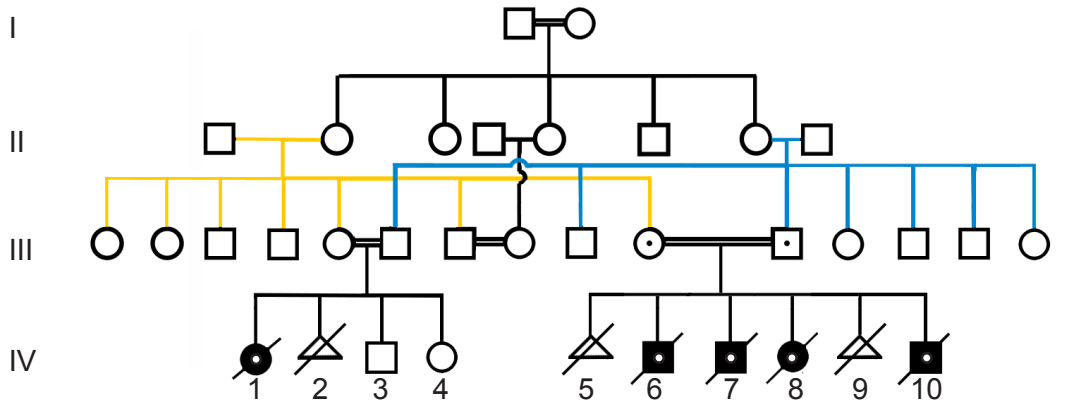

FAMILY B
PAKISTAN

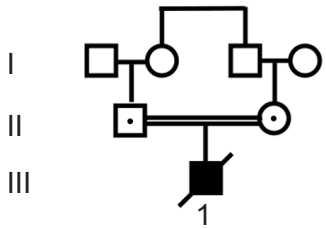

c.[68G>T];[68G>T]
p.[Gly23Val];[Gly23Val]

FAMILY C
PAKISTAN

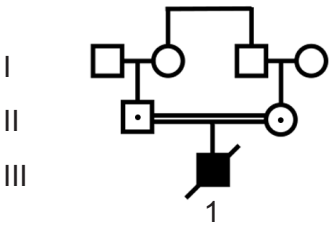

c.[68G>T];[68G>T]
p.[Gly23Val];[Gly23Val]

FAMILY D
SAUDI ARABIA

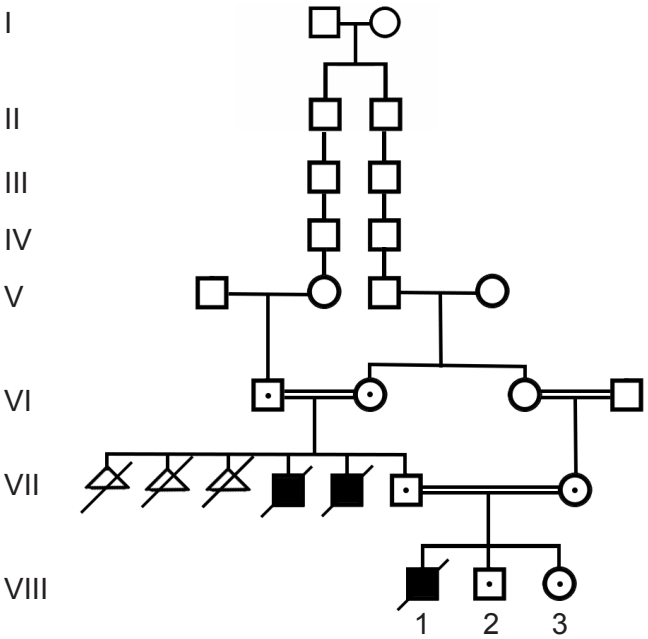

c.[68dupG];[68dupG]
p.[Leu24Profs*55];[Leu24Profs*55]

Figure S2: PLAA is essential for mammalian development.

Related to **Figure 2.** *Plaa*$^{+/tm1(NCOM)Cmhd}$ C2 (Nagy) embryonic stem cells, which have insertion of NorCOMM cassette pNTARU creating a 918bp deletion, removing Exon2 of *Plaa,* and inserting a LacZ reporter gene, were injected into C57BL/6J blastocysts and implanted into a recipient C57BL/6J female. These were backcrossed onto C57BL/6J, then subsequently to CD1, and no differences in survival or gross phenotypes were observed on the two backgrounds studied. (**A**) Schematic of the NORCOMM *Plaa*$^{-}$ deletion allele (*Plaa*$^{-}$*;* MGI:104810), showing replacement of Exon 2 (ENSMUSE00001223836) with a splice acceptor (SA), a self-cleaving peptide (T2A), LacZ gene allowing readout of *Plaa* expression pattern, followed by a strong stop (pA). Position of the human p.Gly23Val mutation is shown as an asterisk in the first exon. (**B**) No PLAA protein remains in *Plaa*$^{-/-}$ MEFs. (**C**) E11.5 LacZ stained *Plaa*$^{+/-}$ embryo, showing ubiquitous expression of the *LacZ* reporter. **(D)** Immunocytochemistry staining reveals PLAA is ubiquitously localized throughout the cell, in both the cytoplasm and the nucleus. The staining is absent in *Plaa*$^{-/-}$ confirming specificity. (**E**) Most *Plaa*$^{-/-}$ embryos die before E15.5 (**Table S3**), and those that survive are smaller, anemic and display a curved body axis. Scale bars represent 1mm (**C**, **E**) or 10 μm (**D**).

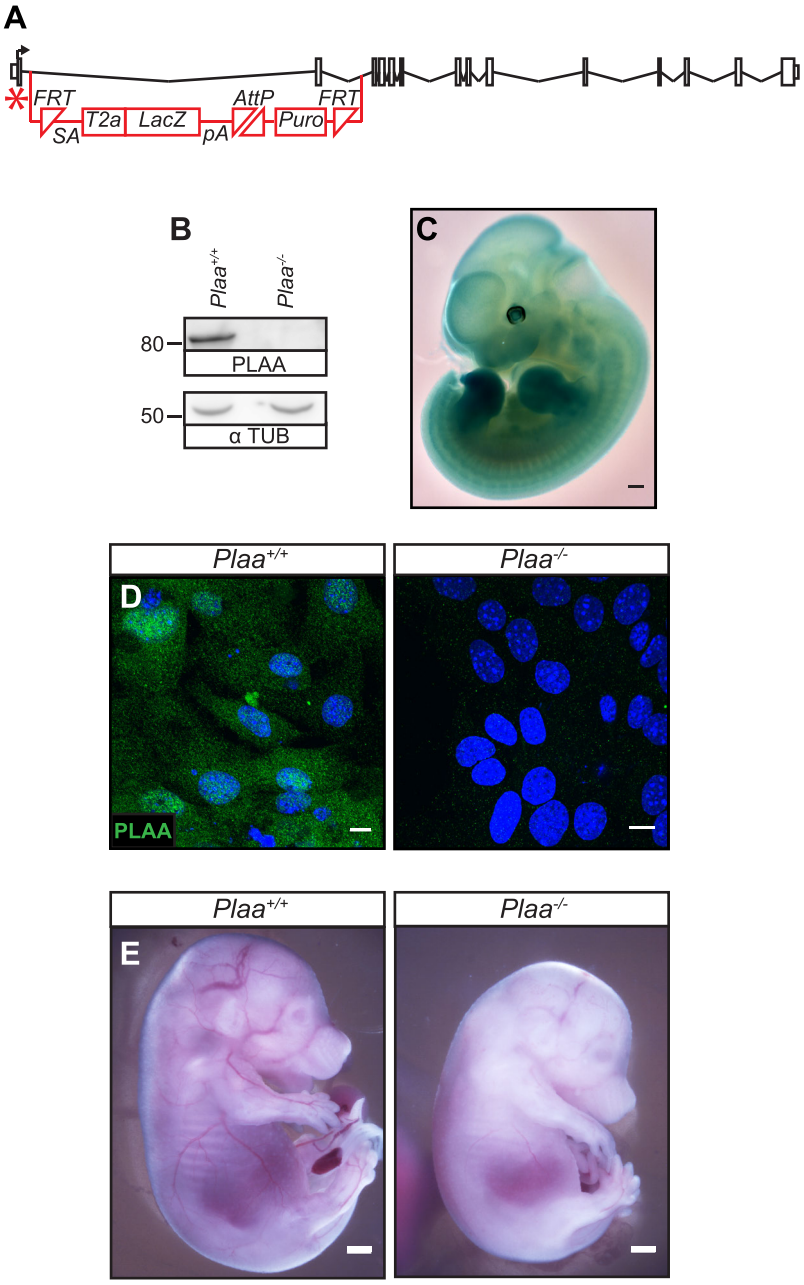
A
FRT
SA
T2a
LacZ
pA
AttP
Puro
FRT
B
Plaa+/+
Plaa-/-
80
PLAA
50
α TUB
C
Plaa+/+
Plaa-/-
D
PLAA
Plaa+/+
Plaa-/-
E

Figure S3: PLAA is not required for normal early endosome or lysosomal morphology. Related to **Figure 2**. (**A**) qRT-PCR depicts no change in transcription of mitophagy-associated genes (*Cox1, Mfn1* and *Atad1*), slight reduction/no change in ERAD genes (*Hsp90b, Hspa5, Vimp1*) and a reduction in expression of *Ubb*, one of several ubiquitin-encoding genes in *Plaa*$^{-/-}$ embryos, suggesting mitophagy, ERAD and UPS transcriptional signatures are not increased upon *Plaa* deletion. n = 5 *Plaa*$^{-/-}$ embryos, n = 4 *Plaa*$^{-/-}$ embryos (**B - E**) Early endosome number and localization is unchanged (marked by EEA1, quantified in **D** and **E**) and lysosomal compartments are grossly normal in *Plaa*$^{-/-}$ MEFs (LAMP1 (**C**)). (**F**) Internalization of DOP-Flag into the lumen of Rab5^{Q79L} enlarged endosomes upon addition of ligand DPDPE is disrupted in *Plaa* null MEFs (quantified in (**G**). Scale bars represent 10 μm. Error bars represent SEM. $P < 0.05$, **, $P < 0.01$, ns not significant. Student's t-test. N = 3 MEF lines per genotype.

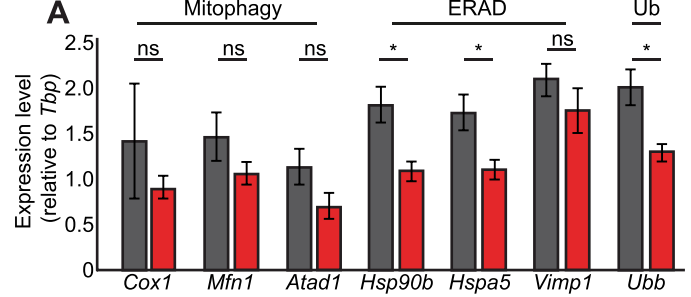
A
Mitophagy
ERAD
Ub
ns
ns
ns
*
*
ns
*
Expression level (relative to Tbp)
2.5
2.0
1.5
1.0
0.5
0
Cox1
Mfn1
Atad1
Hsp90b
Hspa5
Vimp1
Ubb

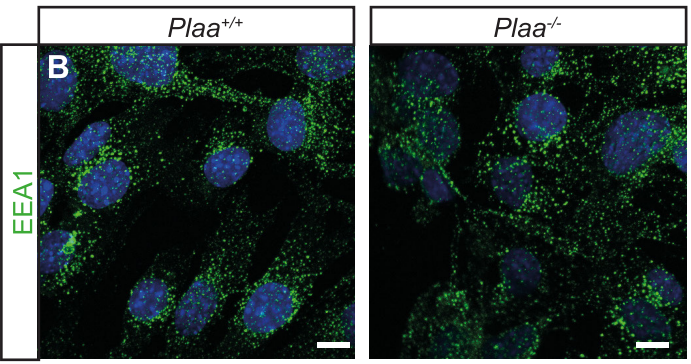
Plaa+/+
Plaa-/-
B
EEA1

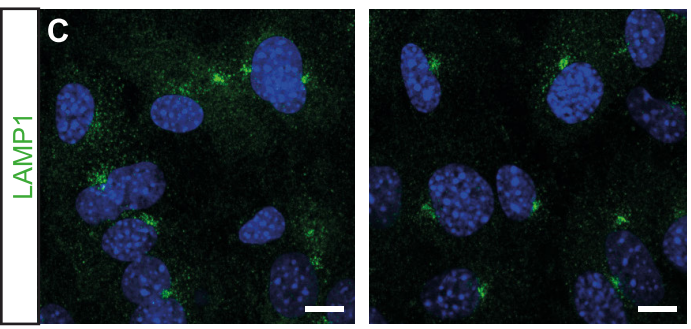
C
LAMP1

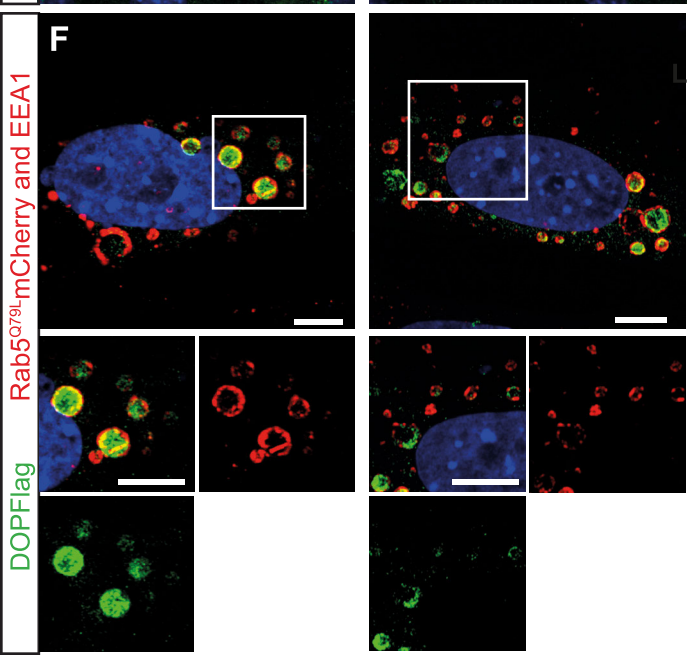
F
Rab5Q79L-mCherry and EEA1
DOPFlag

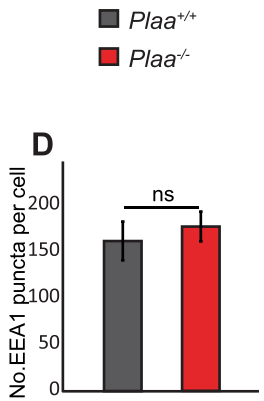
Plaa+/+
Plaa-/-
D
No.EEA1 puncta per cell
200
150
100
50
0
ns

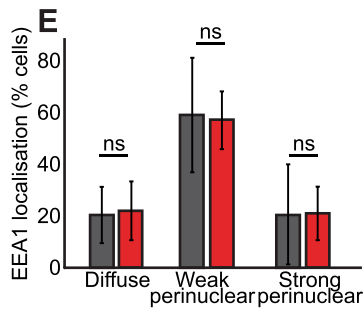
E
EEA1 localisation (% cells)
80
60
40
20
0
ns
ns
ns
Diffuse
Weak perinuclear
Strong perinuclear

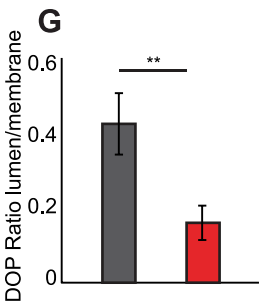
G
DOP Ratio lumen/membrane
0.6
0.4
0.2
0
**

Figure S4: Similar to PLAAND affected individuals, *Plaa*$^{G23V/G23V}$ and *Plaa*$^{G23V/-}$ mice exhibit growth retardation and neuromuscular weakness.

Related to **Figure 2**. (**A**) Schematic strategy for gene editing using CRISPR-CAS9 nickase system to generate the c.68G>T disease mutation in mouse *Plaa* using homology directed repair. Briefly, guide RNA targeting sequences either side of the c.68G (**Table S9**) were cloned into pX335-U6-Chimeric_BB-CBh-hSpCas9n(D10A) (Addgene Plasmid #42335), which encodes nickase Cas9 and together with a ssDNA repair template homologous to 100bp either side of c.68G, with the c.68G>T change introduced (**Table S9**) were pronuclear injected into blastocysts, which were implanted into recipient C57BL/6J females. From one round of injection, 33 animals were born, of which 3 had solely the c.68G>T change. The nature of the mutation was confirmed by Sanger sequencing. Allele symbol: *Plaa*^{em1Pmi} MGI:5828117. (**B**) Sequencing confirming precise editing to the disease mutation (red box) in a *Plaa*$^{G23V/G23V}$ mutant mouse. (**C**) *Plaa*$^{G23V/-}$ mutants have reduced body weight at P14. *Plaa*$^{G23V/G23V}$ mice are normal weight at P14, weigh significantly less at 4 weeks, then catch up to control littermates by 8 weeks. n>3 per genotype. * $P < 0.05$ ** $P < 0.01$, Students t-test. Error bars represent SEM. (**D**) *Plaa*$^{G23V/G23V}$ mice show pronounced kyphosis indicative of neuromuscular weakness.

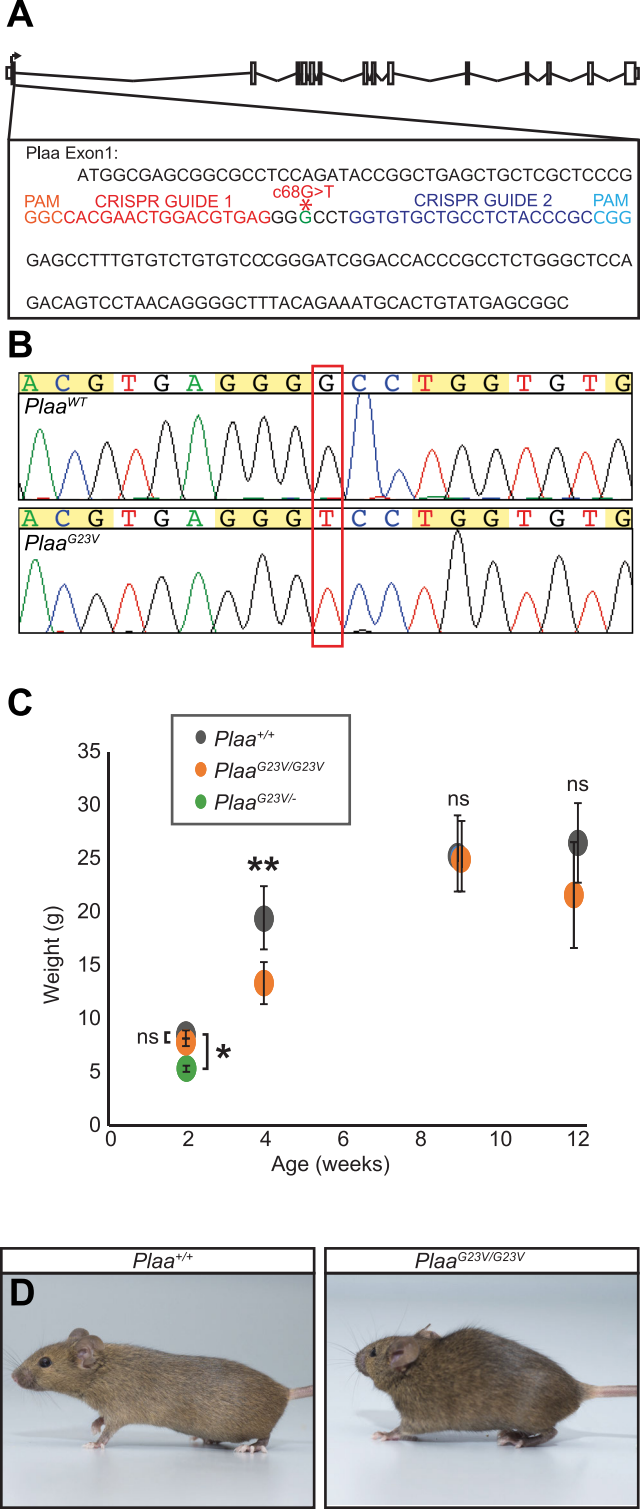
A
Plaa Exon1:
ATGGCGAGCGGCGCCTCCAGATACCGGCTGAGCTGCTCGCTCCCG
PAM
CRISPR GUIDE 1
c68G>T
CRISPR GUIDE 2
PAM
GGCCACGAACTGGACGTGAGGGGCCTGGTGTGCTGCCTCTACCCGCCGG
GAGCCTTTGTGTCTGTGTCCCGGGATCGGACCACCCGCCTCTGGGCTCCA
GACAGTCCTAACAGGGGCTTTACAGAAATGCACTGTATGAGCGGC
B
Plaa^WT
Plaa^G23V
C
Plaa+/+
Plaa^G23V/G23V
Plaa^G23V/-
Weight (g)
Age (weeks)
ns
**
*
D
Plaa+/+
Plaa^G23V/G23V

Figure S5: *Plaa*$^{G23V/G23V}$ and *Plaa*$^{G23V/-}$ mice display early-onset kinetic tremor, disrupted cerebellar morphology and reactive gliosis.

Related to **Figure 4**. (**A - B**) Histological analyses of *Plaa*$^{G23V/G23V}$ cerebella at 3 months and *Plaa*$^{G23V/-}$ cerebella at P20, show *Plaa*$^{G23V/-}$ mice also have significantly smaller cerebella relative to the whole brain at P14 (**C**), with a disrupted foliation pattern. (**D**) *Plaa*$^{G23V/-}$ mice also display early-onset kinetic tremor with postural aspect, detectable by eye from P7 and with this assay from before P14. To measure tremor, mice were placed in a clear Perspex tube suspended inside a box on elasticated bungees mounted with a PZT film sensor LDT0-028 sensor to detect movement. A camera allowed visualization of the mouse during the experiment. Mice were allowed to acclimatize to the tube for 10 minutes before readings were taken. (**E - H**) Microarray analysis of RNA from *Plaa*$^{+/+}$ and *Plaa*$^{G23V/G23V}$ cerebella at 3 months revealed specific signature of down-regulation of Purkinje cell markers and up-regulation of reactive gliosis markers, with no change in the proteins shown to be upregulated by proteomic analysis (**Figure 4G**), confirmed here by qRT-PCR (**E, F, G**). (**H**) Western blot confirming the upregulation of AP4S1 and SNAP25 seen by proteomic analysis (**Figure 4G**). Graphs to the right show densitometry of AP4S1 and SNAP25 relative to α-tubulin (α-TUB). (**I**) Synaptic preparations from *Plaa*$^{+/+}$ and *Plaa*$^{G23V/G23V}$ cerebella again confirm the upregulation of SNAP25 (quantified in **J**), while also showing PLAA is present in both the cytoplasmic and synaptic preps. Levels of free and poly-ubiquitin in the synapse are unchanged (quantified in **K**). Error bars represent SEM, * $P < 0.05$, ** $P < 0.01$, *** $P < 0.01$, Student's t-test. Scale bars represent 500μm.

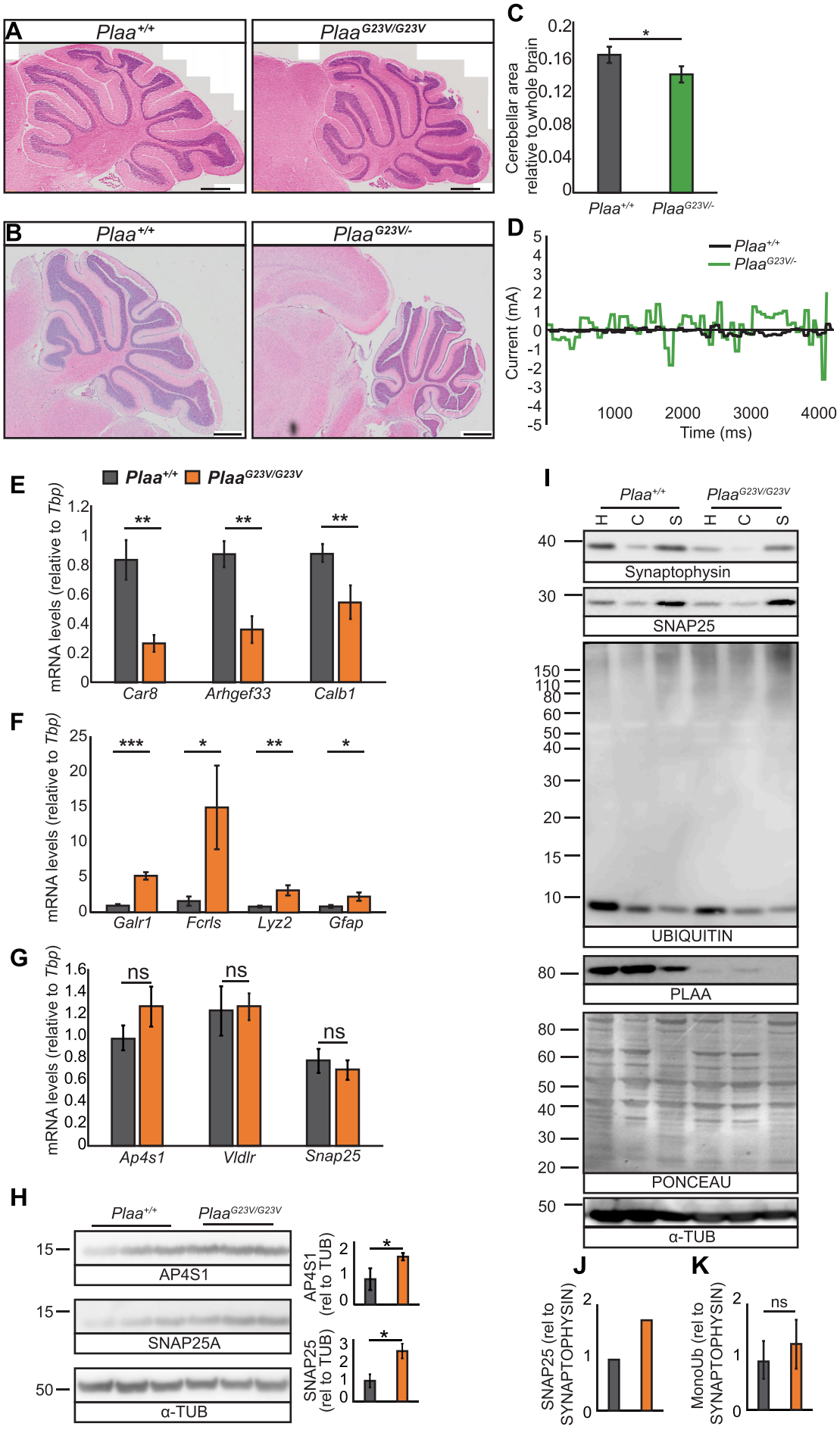
A
Plaa+/+
PlaaG23V/G23V
B
Plaa+/+
PlaaG23V/-
C
Cerebellar area relative to whole brain
0.2
0.16
0.12
0.08
0.04
0
*
Plaa+/+
PlaaG23V/-
D
Plaa+/+
PlaaG23V/-
Current (mA)
5
4
3
2
1
0
-1
-2
-3
-4
-5
1000
2000
3000
4000
Time (ms)
E
Plaa+/+
PlaaG23V/G23V
mRNA levels (relative to Tbp)
1.2
1
0.8
0.6
0.4
0.2
0
**
**
**
Car8
Arhgef33
Calb1
F
mRNA levels (relative to Tbp)
25
20
15
10
5
0
***
*
**
*
Galr1
Fcrls
Lyz2
Gfap
G
mRNA levels (relative to Tbp)
1.6
1.4
1.2
1.0
0.8
0.6
0.4
0.2
0
ns
ns
ns
Ap4s1
Vldlr
Snap25
H
Plaa+/+
PlaaG23V/G23V
15
AP4S1
15
SNAP25A
50
α-TUB
AP4S1 (rel to TUB)
2
1
0
*
SNAP25 (rel to TUB)
3
2
1
0
*
I
Plaa+/+
PlaaG23V/G23V
H
C
S
H
C
S
40
Synaptophysin
30
SNAP25
150
110
80
60
50
40
30
20
15
10
UBIQUITIN
80
PLAA
80
60
50
40
30
20
PONCEAU
50
α-TUB
J
SNAP25 (rel to SYNAPTOPHYSIN)
2
1
0
K
MonoUb (rel to SYNAPTOPHYSIN)
2
1
0
ns

Figure S6: Loss of PLAA function in NMJs decreases pool of recycling/reserve SVs with accumulation of enlarged endosomal structures with conspicuous neurofilament accumulations in mutant synaptic boutons.

Related to **Figure 5.** (**A**) NMJs from 3 month old *Plaa*$^{G23V/-}$ mutant Tibialis Anterior (TA – hindlimb), Adductor Auris Longus (AAL – cranial) and transverse abdominus (TVA – abdominal muscles) stained with Neurofilament (NF), Synaptic Vesicle 2 (SV2) and Bungarotoxin (BTX) showing abnormal sprouting and accumulations, particularly evident in the NMJs innervating cranial muscles, quantified in **B** and **C**. Briefly, muscles were dissected and fixed in 4% PFA (Electron Microscopy Science) in PBS for 15 min. Post-synaptic acetylcholine receptors (AChRs) were labelled with α-bungarotoxin (BTX) for 30 min. Muscles were permeabilised in 2% Triton X-100 in PBS for 30 min, then blocked in 4% bovine serum albumin (BSA)/1% Triton X-100 in PBS for 30 min before incubation overnight with immunoreagents (**Tables S7, S8**). Muscles were then whole-mounted in fluorescent mounting media. All quantification was performed by visual inspection of the muscle. (**D-G**) NMJs labelled with antibodies against only NF (green, **D,F**) and BTX (red) from AAL muscle from wild type and *Plaa*$^{G23V/-}$ mice at P15. The percentage of NMJs with accumulations (**E**) and the number of sprouts per NMJ (**G**) is quantified (n = 3 mice/ genotype). (**H**) Transmission electron microscopy of wild type littermate and *Plaa*$^{G23V/G23}$ mutant synaptic boutons from NMJs on LAL cranial muscles at 3 months. While control NMJs have uniformly abundant pools of SVs throughout the bouton (left hand panels and **Figure 5J**, central pools of SVs are missing in *Plaa*$^{G23V/G23V}$ mutant boutons (center and right hand panels and **Figure 5K-M**). Remaining SVs are found either restricted to periphery clustered at active zones and/or denuded, despite being adjacent to well defined post-synaptic densities and folds. Prominent accumulations of enlarged endosomal structures and vacuolated structures are observed in mutant boutons. Central neurofilament accumulations (asterisk) are also apparent. For transmission electron microscopy, muscle samples were immersed in modified Karnovsky's fixative (2.5% glutaraldehyde, 2% paraformaldehyde in 0.1M sodium cacodylate buffer pH7.4 with 0.05% calcium chloride) at 4^{o}C overnight, rinsed in 0.1M sodium cacodylate buffer pH7.4 with 0.05% calcium chloride before further NMJ sub-dissection, then post-fixed in 1% osmium tetroxide. Samples were dehydrated in graded acetone then progressively embedded in Epoxy embedding resin (medium: TAAB Lab. Equip). Ultrathin sections (~70 nm) were cut and stained with 2% uranyl acetate followed by Leica Lead stain (Leica) and viewed using a Philips CM 100 Compustage (FEI) Transmission Electron Microscope with an AMT CCD camera (Deben). Scale bar represents 60μm (**A**), 50μm (**D**). 20μm (**F**) and 500 nm (**H**) Error bars represent SEM. * $P < 0.05$, Mann Whitney U test, n = 3 mice per genotype.

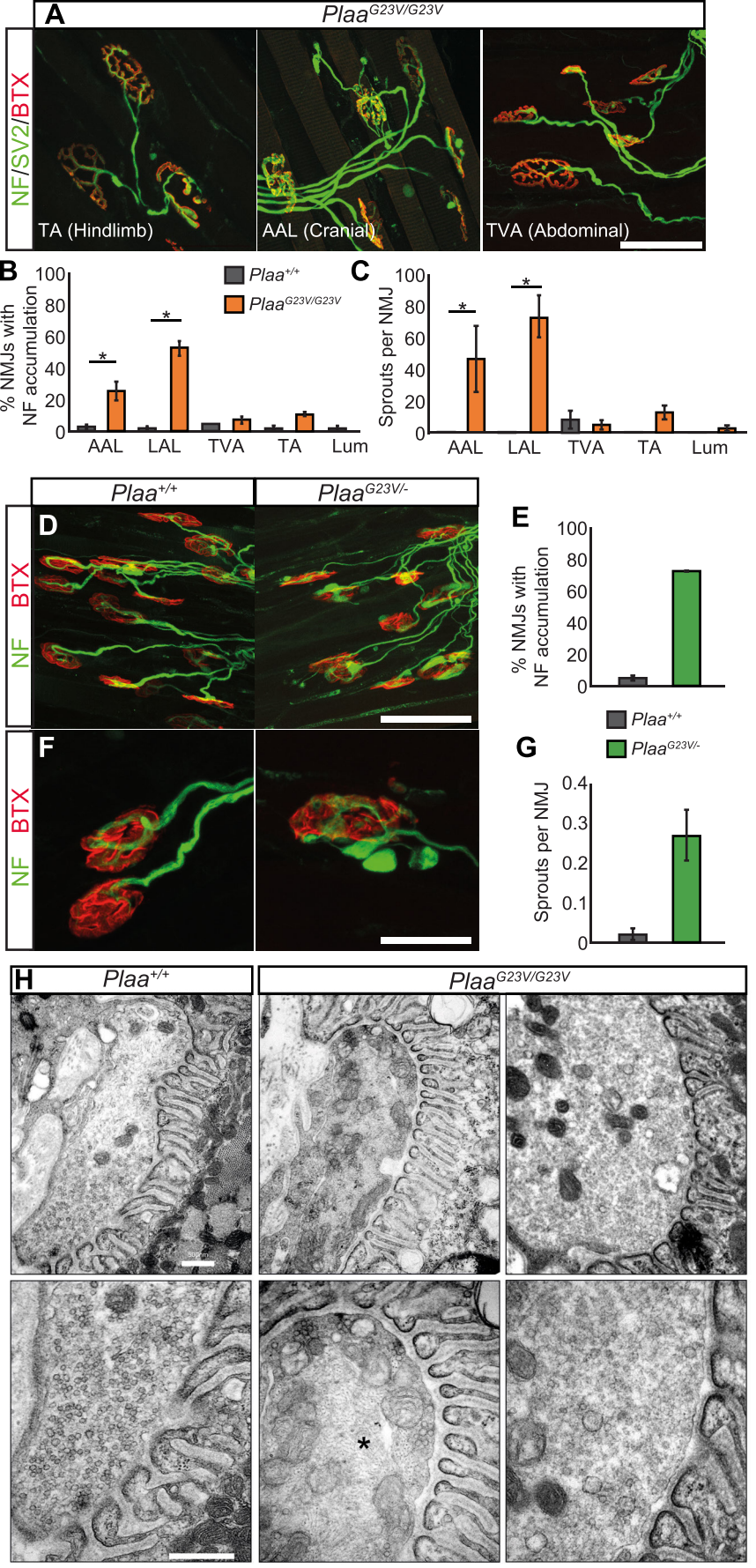
A
Plaa G23V/G23V
NF/SV2/BTX
TA (Hindlimb)
AAL (Cranial)
TVA (Abdominal)
B
% NMJs with NF accumulation
Plaa +/+
Plaa G23V/G23V
AAL
LAL
TVA
TA
Lum
C
Sprouts per NMJ
D
Plaa +/+
Plaa G23V/-
NF BTX
E
F
G
H

Figure S7: Reduction in PLAA disrupts synaptic function at NMJs.

Related to **Figure 6**. (**A**) Muscle fiber diameter is significantly reduced in *Plaa*$^{G23V/G23V}$ LAL muscles demonstrating muscle atrophy, perhaps due to reduced movement. (**B**) Endplate length is increased in *Plaa*$^{G23V/G23V}$ LAL muscles. (**C-E**) MEPP amplitude and rise time is unaffected in *Plaa*$^{G23V/G23V}$ LAL NMJs, however the half decay time is increased, consistent with a longer membrane time constant typically associated with atrophic muscle fibers. (**F-I**) However, of the LAL muscles fibers that responded (**Figure 6D**), EPPs appeared normal with similar amplitude, half decay and rise time to controls. All animals on this figure were 7 months old; n=2 control (*Plaa*$^{G23V/+}$) and n=4 *Plaa*$^{G23V/G23V}$, Student's T-test, * $P < 0.05$, ** $P < 0.01$, *** $P < 0.001$.

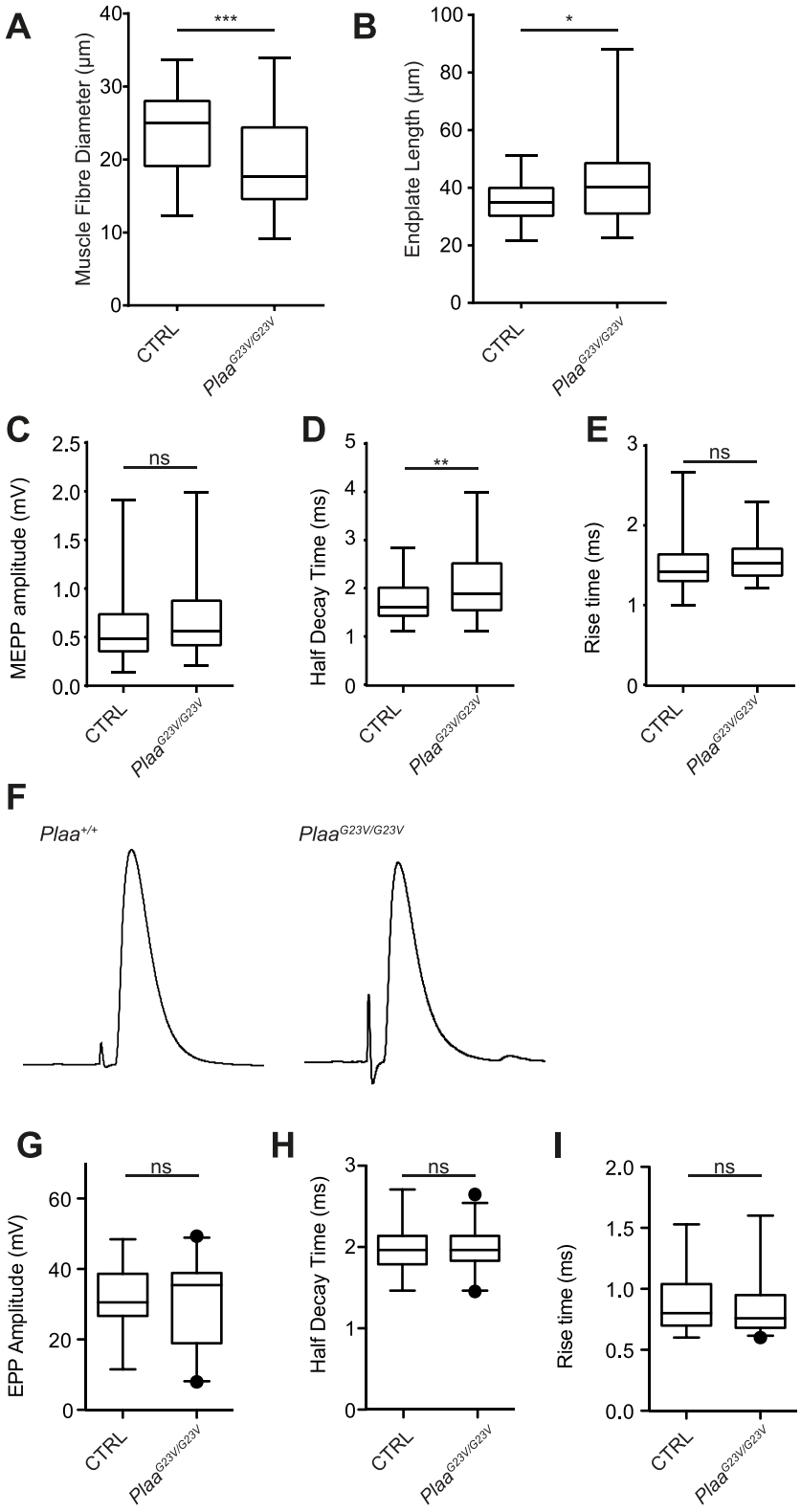
A
Muscle Fibre Diameter (µm)
***
CTRL
Plaa G23V/G23V
B
Endplate Length (µm)
*
C
MEPP amplitude (mV)
ns
D
Half Decay Time (ms)
**
E
Rise time (ms)
ns
F
Plaa +/+
Plaa G23V/G23V
G
EPP Amplitude (mV)
ns
H
Half Decay Time (ms)
ns
I
Rise time (ms)
ns

Figure S8: p62 reroutes accumulated K63-linked polyUb substrates for autophagy in the absence of PLAA.

Related to **Figure 7**. (**A**) Proteasome activity was assessed in freshly isolated cerebella lysates with AMC-labelled trypsin or chemotypsin substrates (+/- inhibitor MG132). No impairment in proteasomal activity in *Plaa*$^{G23V/G23V}$ brain extracts was observed, similar to null cells (**Figure 2B**). (**B**) No compensatory increase in ubiquitin or ERAD genes was observed. (**C**) Confirmation of the specific accumulation of K63-ubiquitylated cargo in *Plaa*$^{G23V/-}$ cerebella upon affinity purification using the K63-specific ubiquitin binding domain (UBD) of Eps15 using K63 and K48-ubiquitin-specific antibodies. (**D**) Affinity purification of pan-ubiquitylated substrates using Ubqln1 UBD revealed no accumulation of total poly-ubiquitylated proteins in *Plaa*$^{G23V/-}$ cerebella, presumably as other non-K63-linked chains are masking the increase seen by K63-ubiquitin specific pulldown. (**E**) Pulldown of K48-ubiquitylated proteins revealed a very slight accumulation of K48-ubiquitylated proteins in *Plaa*$^{G23V/-}$ cerebella using Fam63 UBD. **(F)** To assay induction of autophagic responses under nutrient deprivation *Plaa*$^{+/+}$ and *Plaa*$^{-/-}$ MEFs were treated with BAFA1, starvation media EBSS or both. *Plaa*$^{-/-}$ MEFs show response to autophagy induction by starvation, as indicated by an increased LC3-II, suggesting the core autophagy machinery is intact. (**G**) A subset of the p62 foci colocalize with aberrant HRS positive endosomal structures in *Plaa*$^{-/-}$ MEFs. Enlarged panels are shown to the right and in **Figure 7E**. (**H**) Transfection of MEFs with LC3-RFP-GFP autophagy reporter reveals the total number of LC3+ foci are increased in *Plaa*$^{-/-}$ MEFs (**I**). However, the ratio of mature autophagolysosomes (RFP only) to immature autophagosomes (double RFP/GFP- yellow) is unchanged (**J**), suggesting increased basal autophagy, without impairing fusion events in *Plaa*$^{-/-}$ MEFs. n=3 per genotype. Scale bar represents 10μm. * $P < 0.05$. Student's t-test. Error bars represent SEM, n = 3 MEF lines per genotype. Blots representative of n > 3 per genotype.

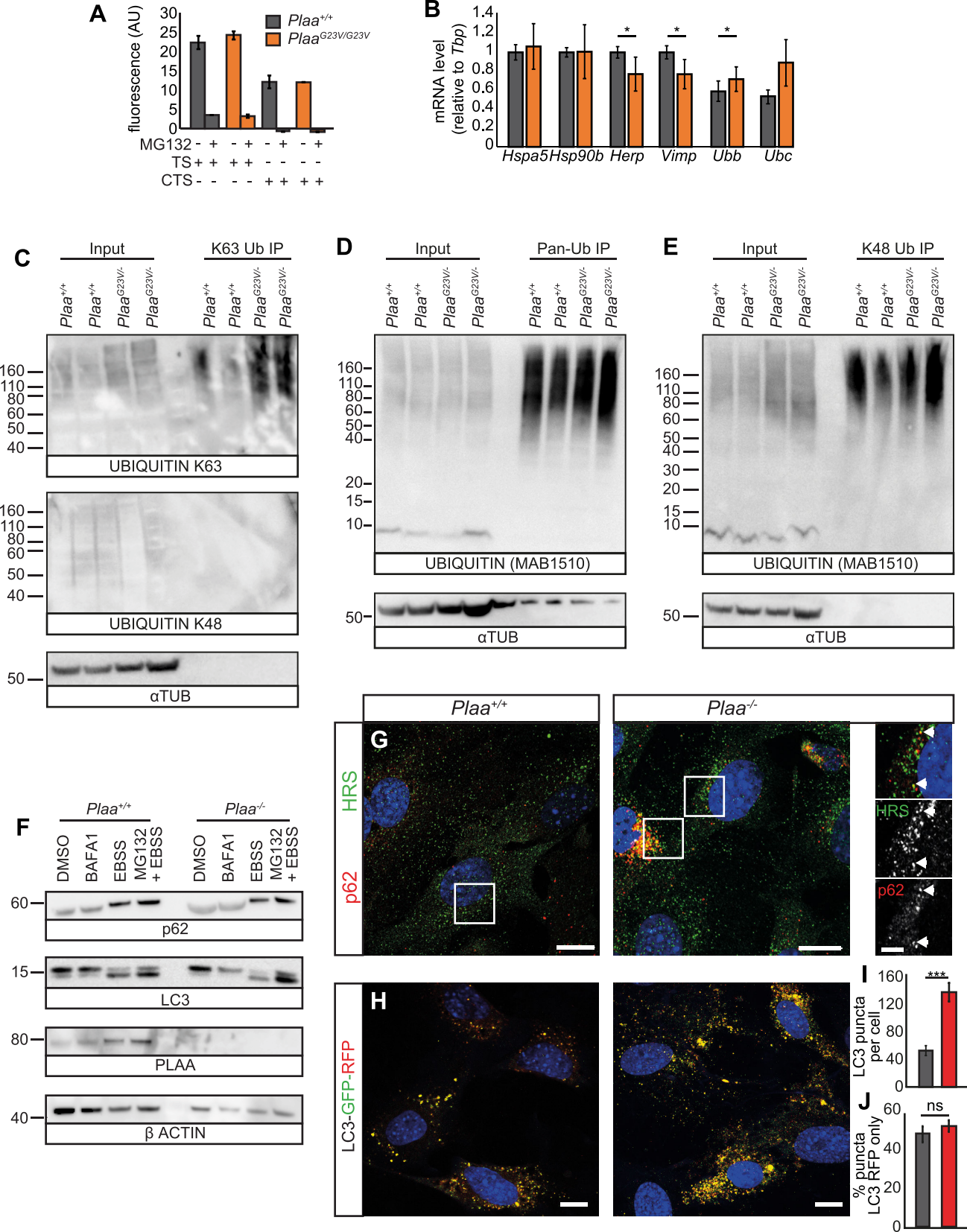
A
fluorescence (AU)
Plaa+/+
PlaaG23V/G23V
MG132
TS
CTS
B
mRNA level (relative to Tbp)
Hspa5
Hsp90b
Herp
Vimp
Ubb
Ubc
C
Input
K63 Ub IP
UBIQUITIN K63
UBIQUITIN K48
αTUB
D
Input
Pan-Ub IP
UBIQUITIN (MAB1510)
αTUB
E
Input
K48 Ub IP
UBIQUITIN (MAB1510)
αTUB
F
DMSO
BAFA1
EBSS
MG132 + EBSS
p62
LC3
PLAA
β ACTIN
G
HRS
p62
H
LC3-GFP-RFP
I
LC3 puncta per cell
***
J
% puncta LC3 RFP only
ns

Figure S9: cPLA2 activity is unchanged in *Plaa*$^{G23V/-}$ brains.

(**A**) PLAA's implication in phospholipase biology has come from use of a 19 amino acid peptide fragment from PLAA (795aa protein), which activates phospholipase A_2 in a dose-dependent manner and bears considerable homology to melittin (bee venom)[91]. Activation of PLA2 leads to hydrolysis of phospholipids generating the precursor for eicosanoids, which are involved in diverse signaling cascades, primarily through their interaction with cellular receptors and ion channels. Whether endogenous PLAA directly activates cytoplasmic phospholipase A2 activity under physiological conditions remains unclear, and whether any effect could involve PLAA modulation of Ub signaling of additional intermediates has yet to be determined. (**B**,**C**) PLA2 activity in membrane extracts from P15 *Plaa*$^{G23V/-}$ brains were analyzed with fluorescent (**B**) and colorimetric (**C**) substrates. Neither showed significant change in cPLA2 activity in severely symptomatic brains, suggesting disrupted phospholipid signaling is not the primary cause of defects observed in early symptomatic neurons.

Brains were cut into 2mm cubes, rinsed in PBS and homogenised in 50mM Tris pH8.0, 1mM EDTA, 1mM EGTA, 20% glycerol plus HALT protease inhibitor (Pierce). Lysates were clarified at 10,000g for 10 minutes, and membrane fractionation was performed by spinning the supernatant at 100,000g for 1 hour at 4°C. The pellet was resuspended in homogenisation buffer plus 0.1% Triton X to give the membrane fraction. PLA2 activity was assayed with EnzChek Phospholipase A2 Assay Kit (Thermofisher) (**B**), or cPLA2 Assay Kit (Cayman Chemicals) (**C**) according to manufacturers' instructions.

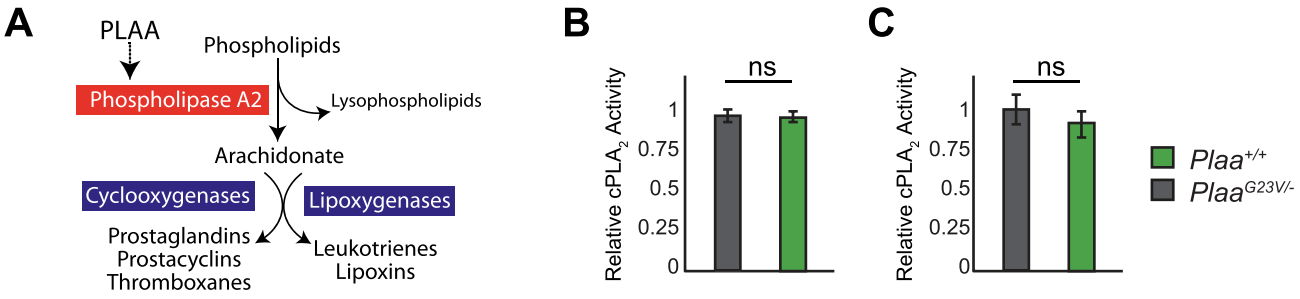
A
PLAA
Phospholipids
Phospholipase A2
Lysophospholipids
Arachidonate
Cyclooxygenases
Lipoxygenases
Prostaglandins
Prostacyclins
Thromboxanes
Leukotrienes
Lipoxins
B
ns
Relative cPLA2 Activity
1
0.75
0.5
0.25
0
C
ns
Relative cPLA2 Activity
1
0.75
0.5
0.25
0
Plaa+/+
PlaaG23V/-

Supplemental Table S1. Detailed clinical table. Related to Figure 1.

Patient #		A-IV-6	A-IV-7	A-IV-8	Patient #	A-IV-10	A-IV-1	B-III-1	C-III-1
Gender		M	M	F	Gender	M	F	M	M
Diagnosis age		At birth	At birth	1st week	Diagnosis age	At birth	1st week	1st week	At birth
Age at death		12 days	1.5 years	2.3 years	Age at death	live at 0.5 yea	1.2 years	5 years	6 years
Clinical feature	HPO #				**Clinical feature**				
Central nervous system					*Central nervous system*				
Abnormal cortical gyration	HP:0002536	N.E.	+	+	Abnormal cortical gyration	+	+	+	N.E.
Abnormality of the cerebellum	HP:0001317	N.E.	N.E.	N.E.	Abnormality of the cerebellum	N.E.	N.E.	+	+
Bulbar symptoms	HP:0002483	+	+	N.E.	Bulbar symptoms	+	+	N.E.	N.E.
Central hypotonia	HP:0011398	+	+	N.E.	Central hypotonia	+	+	N.E.	+
Delayed myelination	HP:0012448	N.E.	+	+	Delayed myelination	N.E.	-	N.E.	+
Cessation of head growth	HP:0004485	N.E.	+	+	Cessation of head growth	+	+	+	+
Cognitive impairment	HP:0100543	+	+	+	Cognitive impairment	+	+	+	+
Generalized seizures	HP:0002197	N.E.	N.E.	+	Generalized seizures	+	+	+	+
Hypertonia	HP:0001276	+	+	N.E.	Hypertonia	+	+	+	+
Hypodysplasia of the corpus callosum	HP:0006849	+	+	+	Hypodysplasia of the corpus callosum	+	N.E.	N.E.	+
Optic atrophy	HP:0000648	N.E.	+	N.E.	Optic atrophy	N.E.	N.E.	+	+
Nystagmus	HP:0000639	N.E.	N.E.	+	Nystagmus	+	+	+	N.E.
Periventricular cysts	HP:0007109	+	N.E.	N.E.	Periventricular cysts	N.E.	N.E.	N.E.	N.E.
Development					*Development*				
Gross motor		N.E.	Absent	Absent	Gross motor	Absent	Absent	Absent	Absent
Fine motor		N.E.	Absent	Absent	Fine motor	Absent	Absent	Absent	Absent
Language		N.E.	Absent	Absent	Language	Absent	Absent	Absent	Absent
Social		N.E.	Absent	Absent	Social	Absent	Absent	Absent	Absent
Other					*Other*				
Congenital hypothyroidism	HP:0000851	+	-	-	Congenital hypothyroidism	-	-	-	-
Edema of the dorsum of feet	HP:0012098	-	+	-	Edema of the dorsum of feet	+	-	+	+
Edema of the dorsum of hands	HP:0007514	-	-	-	Edema of the dorsum of hands	+	-	-	+
Postaxial polydactyly	HP:0100259	+	+	-	Postaxial polydactyly	-	-	-	-
Coarse facies	HP:0000280	+	+	+	Coarse facies	+	+	+	+
Hirsutism	HP:0001007	+	N.E.	N.E.	Hirsutism	+	N.E.	N.E.	N.E.

Table S2. List of exome variants identified genes in candidate interval in Family A. Related to **Figure 1.**

SPLICE REGION VARIANT

Position	Change	Filter	Score	Depth	Genotype	gene	transcript	Effect	AA change	Grantham score	dbsnp	PolyPhen	SIFT
9:14806848	C>A	.	222	42	HOMO	*FREM1*	ENST00000380881	splice_region_variant&intron_variant			rs10810249		
9:14806848	C>A	.	222	42	HOMO	*FREM1*	ENST00000380875	splice_region_variant&intron_variant&NMD_transcript_variant			rs10810249		
9:14806848	C>A	.	222	42	HOMO	*FREM1*	ENST00000380880	splice_region_variant&intron_variant			rs10810249		
9:14806848	C>A	.	222	42	HOMO	*FREM1*	NM_144966.5	splice_region_variant&intron_variant			rs10810249		

MISSENSE VARIANT

Position	Change	Filter	Score	Depth	Genotype	gene	transcript	Effect	AA change	Grantham score	dbsnp	PolyPhen	SIFT
9:14722477	G>C	.	219	80	HOMO	*CER1*	NM_005454.2	missense_variant	A/G	60	rs3747532	benign(0)	tolerated(1)
9:14819370	G>T	.	222	142	HOMO	*FREM1*	ENST00000380881	missense_variant	S/Y	144	rs7023244	probably_damaging(0.924)	deleterious(0.01)
9:14819370	G>T	.	222	142	HOMO	*FREM1*	ENST00000380875	missense_variant&NMD_transcript_variant	S/Y	144	rs7023244	probably_damaging(0.975)	deleterious(0.01)
9:14819370	G>T	.	222	142	HOMO	*FREM1*	ENST00000380880	missense_variant	S/Y	144	rs7023244	probably_damaging(0.924)	deleterious(0.01)
9:14819370	G>T	.	222	142	HOMO	*FREM1*	NM_144966.5	missense_variant	S/Y	144	rs7023244	probably_damaging(0.924)	deleterious(0.01)
9:14846036	C>G	.	222	127	HOMO	*FREM1*	ENST00000380881	missense_variant	V/L	32	rs2779500	benign(0.029)	tolerated(0.1)
9:14846036	C>G	.	222	127	HOMO	*FREM1*	ENST00000380875	missense_variant&NMD_transcript_variant	V/L	32	rs2779500	benign(0.03)	tolerated(0.18)
9:14846036	C>G	.	222	127	HOMO	*FREM1*	ENST00000380880	missense_variant	V/L	32	rs2779500	benign(0.029)	tolerated(0.1)
9:14846036	C>G	.	222	127	HOMO	*FREM1*	NM_144966.5	missense_variant	V/L	32	rs2779500	benign(0.029)	tolerated(0.1)
9:21187121	T>A	.	222	230	HOMO	*IFNA4*	NM_021068.2	missense_variant	E/V	121	rs113045626	benign(0.057)	tolerated(0.14)
9:21187311	C>T	.	222	86	HOMO	*IFNA4*	NM_021068.2	missense_variant	A/T	58	rs1062571	benign(0.04)	tolerated(0.19)
9:21206763	G>T	.	222	105	HOMO	*IFNA10*	NM_002171.1	missense_variant	L/I	5	rs56035072	probably_damaging(0.991)	deleterious(0.01)
9:21207000	C>G	.	222	63	HOMO	*IFNA10*	NM_002171.1	missense_variant	G/R	125	rs10113875	benign(0.042)	tolerated(0.55)
9:21207005	C>G	.	222	57	HOMO	*IFNA10*	NM_002171.1	missense_variant	S/T	58	rs10113876	benign(0.348)	tolerated(0.52)
9:21227622	A>C	.	221	105	HOMO	*IFNA17*	NM_021268.2	missense_variant	I/R	97	rs9298814	benign(0)	tolerated(1)
9:21228040	C>G	.	222	111	HOMO	*IFNA17*	NM_021268.2	missense_variant	G/R	125	rs12552812	benign(0.001)	tolerated(1)
9:25677953	T>C	.	51.3	7	HOMO	*TUSC1*	NM_001004125.2	missense_variant	N/D	23	rs34498078	benign(0)	tolerated(1)
9:26946976	C>A	.	98.1	7	HOMO	*PLAA*	ENST00000523212	missense_variant	G/V	109	.	probably_damaging(0.919)	deleterious(0.01)
9:26946976	C>A	.	98.1	7	HOMO	*PLAA*	ENST00000520884	missense_variant	G/V	109	.	probably_damaging(0.991)	deleterious(0.02)
9:26946976	C>A	.	98.1	7	HOMO	*PLAA*	NM_001031689.2	missense_variant	G/V	109	.	probably_damaging(0.991)	deleterious(0.01)
9:27183463	A>C	.	222	169	HOMO	*TEK*	ENST00000406359	missense_variant	Q/P	76	rs682632	benign(0)	tolerated(0.3)
9:27183463	A>C	.	222	169	HOMO	*TEK*	ENST00000519097	missense_variant	Q/P	76	rs682632	benign(0)	tolerated(0.29)
9:27183463	A>C	.	222	169	HOMO	*TEK*	ENST00000519080	missense_variant	Q/P	76	rs682632	benign(0)	tolerated(0.31)
9:27183463	A>C	.	222	169	HOMO	*TEK*	NM_000459.3	missense_variant	Q/P	76	rs682632	benign(0)	tolerated(0.57)
9:27524731	A>G	.	222	146	HOMO	*IFNK*	NM_020124.2	missense_variant	K/E	56	rs700785	benign(0.001)	tolerated(1)

Table S3. Numbers born from *Plaa*$^{+/-}$ X *Plaa*$^{+/-}$ intercrosses.

Age	*Plaa*$^{+/+}$	*Plaa*$^{+/-}$	*Plaa*$^{-/-}$	Chi squared
E11.5	53	110	41	P = 0.2636
E13.5	15	28	5	P = 0.0639
E14.5	32	52	10	P = 0.0034
E15.5	14	22	5	P = 0.1243
Weaning	60	103	0	P < 0.0001

Table S4. Numbers born from *Plaa*$^{+/G23V}$ X *Plaa*$^{+/G23V}$ (genotyped at weaning).

Plaa$^{+/+}$	*Plaa*$^{+/G23V}$	*Plaa*$^{G23V/G23V}$	Chi squared
64	99	49	P = 0.2179

Table S5. Numbers born from *Plaa*$^{+/-}$ X *Plaa*$^{+/G23V}$ (genotyped at ~P14).

Plaa$^{+/+}$	*Plaa*$^{+/-}$	*Plaa*$^{+/G23V}$	*Plaa*$^{G23V/-}$	Chi squared
14	11	8	18	P = 0.2314

Table S7 Primary antibodies

Antigen	Antibody/Clone Name	Host species	Source	Application
a-tubulin	ab4074	Rabbit	Abcam	WB (1:1000)
β-Actin	20536-1-AP	Rabbit	Proteintech Group	WB (1:1000)
AP4S1	ab157573	Mouse	Abcam	WB (1:1000)
CD71	R17217 (FITC conjugated)	Mouse	Molecular Probes	FACS (1:100)
EEA1	3288P	Rabbit	Cell Signalling Technology	IF (1:100)
FLAG	DDK (4C5)	Mouse	Origene	IF (1:500)
GFP	632375	Mouse	Clontech	WB (1:10000)
HA	16B12	Mouse	Biolegend	WB (1:1000)
HRS	ab15539	Rabbit	Abcam	IF (1:100)
LAMP1	ab24170	Rabbit	Abcam	IF (1:1000)
LC3B	L7543	Rabbit	Sigma	WB (1:1000)
Neurofilament	2H3	Mouse	DSHB	IF (1:500)
p62	BML-PW9860-0100	Rabbit	Enzo Life Sciences	IF () WB (1:1000)
p62	GP62-C	Guinea Pig	Progen Biotechnik	IF (1:100)
PLAA	12529-1-AP	Rabbit	Abcam	WB (1:500-1000) IF (1:500)
SNAP25A	3067	Rabbit	Kind gift from Luke Chamberlain	WB (1:1000)
SNAP25	ab5666	Rabbit	Abcam	WB (1:1000)
SV2	SV2	Mouse	DSHB	IF (1:500) WB (1:500)
SYNAPTOPHYSIN	SVP-38	Mouse	Sigma	WB (1:1000)
TER119	TER119 (APC conjugated)	Mouse	Molecular Probes	FACS (1:100)
UBIQUITIN	Z0458	Rabbit	DAKO	WB (1:2,500)
UBIQUITIN	MAB1510	Mouse	EMD Millipore	WB (1:500)
UBIQUITIN-K48	Apu2	Rabbit	EMD Millipore	WB (1:500)
UBIQUITIN-K63	Apu3	Rabbit	EMD Millipore	WB (1:500)
VLDLR	6A6	Mouse	Santa Cruz	WB (1:200)

Table S8 Secondary antibodies

Antigen	Host Species	Dilution	Source	Application
ECL α-Mouse IgG, HRP-conjugated	Sheep	1:7500	GE Healthcare UK Ltd	WB
ECL α-Rabbit IgG, HRP-conjugated	Sheep	1:7500	GE Healthcare UK Ltd	WB
Alexa 488-conjugated-α-Mouse	Donkey	1:500	Molecular Probes	IF
Alexa 594-conjugated-α-Rabbit	Donkey	1:500	Molecular Probes	IF
Alexa 488-conjugated-α-Rabbit	Donkey	1:500	Molecular Probes	IF
Alexa 594-conjugated-α-Guinea Pig	Goat	1:500	Molecular Probes	IF
Alexa 488-conjugated-α-Mouse	Rabbit	1:250	Jackson ImmunoResearch	IF (NMJ wholemount)

Table S9 Primer and Crispr Guide Sequences

Name	Sequence	Notes
713	5’- CGACCCCATGCATCGATGAT -3’	Genotyping *Plaa* $^{-}$ Vector specific primers: Will only amplify from mutant allele
714	5’- CCCGTAGCTCCAATCCTTCC -3’	
705	5’- TGCCCTTTGCTTTCTTGTTT -3’	
706	5’-TGACGGTCCAAAAAGGTTTC -3’	Genotyping *Plaa* $^{-}$: Will not amplify from mutant allele
3F	5’- GGCCTGTGGACGAGTCTC-3’	Genotyping *Plaa* ^{G23V} : Followed by AvaII digestion as c.68G>T change introduces an AvaII site.
2R	5’-GATCCCGGGACACAGACAC-3’	
CRISPR Guide #1	5’-CACGAACTGGACGTGAG-3’	
CRISPR Guide #2	5’-GGTGTGCTGCCTCTACCCGC-3’	
CRISPR Repair Template	5’- CCCGGGGGCCGGGCTCCGGATCCACGCTGGCCATGGCG AGCGGCGCCTCCAGATACCGGCTGAGCTGCTCGCTCCCG GGCCACGAACTGGACGTGAGGG**T**CCTGGTGTGCTGCCTC TACCCGCCGGGAGCCTTTGTGTCTGTGTCCCGGGATCGG ACCACCCGCCTCTGGGCTCCAGACAGGTGAGCGCTGCTA GTCCCG-3’	c.68G>T change highlighted in bold

91. Clark, M.A., Ozgur, L.E., Conway, T.M., Dispoto, J., Crooke, S.T., and Bomalaski, J.S. (1991). Cloning of a phospholipase A2-activating protein. Proceedings of the National Academy of Sciences of the United States of America 88, 5418-5422.